ENGINEERING MATHEMATICS
AND COMPUTING LAB

UNIVERSITÄT
HEIDELBERG
ZUKUNFT
SEIT 1386

Spatial Effect on Separatrix of Two-Cell System and Parameter Sensitivity Analysis

Chen Song, Jonas Roller, Ana Victoria Ponce-Bobadilla, Nicolas Palacio-Escat, Julio Saez-Rodriguez, Vincent Heuveline

Preprint No. 2021-01

Preprint Series of the Engineering Mathematics and Computing Lab (EMCL)

www.emcl.iwr.uni-heidelberg.de

Preprint Series of the Engineering Mathematics and Computing Lab (EMCL)
ISSN 2191–0693
Preprint No. 2021-01

Affiliation of the Authors

Chen Song.[a,b], Jonas Roller[a], Ana Victoria Ponce-Bobadilla[c], Nicolàs Palacio-Escat[c], Julio Saez-Rodriguez[c], Vincent Heuveline[a,b]

[a] *Engineering Mathematics and Computing Lab (EMCL), Interdisciplinary Center for Scientific Computing (IWR), Heidelberg University, Germany*
[b] *Heidelberg Institute for Theoretical Studies(HITS), Germany*
[c] *Institute for Computational Biomedicine, Faculty of Medicine, BIOQUANT-Center, Heidelberg University, Heidelberg, Germany*

Impressum

Heidelberg University
Interdisciplinary Center for Scientific Computing (IWR)
Engineering Mathematics and Computing Lab (EMCL)

Im Neuenheimer Feld 205,
69120 Heidelberg
Germany

Spatial Effect on Separatrix of Two-Cell System and Parameter Sensitivity Analysis

Chen Song, Jonas Roller, Ana Victoria Ponce-Bobadilla, Nicolas Palacio-Escat, Julio Saez-Rodriguez, Vincent Heuveline

April 22, 2021

Abstract

Inflammation in biological tissues follows a dynamical process where upon injury, interactions between cell types and exchange of growth factors occur. Depending on the distribution of different cell types in space, healing or fibrosis occurs. This process is clearly spatially heterogeneous. An existing modeling framework for this process assumes a spatially homogeneous distribution of fibroblasts and macrophages and is therefore unable to capture spatial effects. We extend this framework to obtain a spatially heterogeneous two-cell circuit also containing cell migration, chemotaxis and cytokine diffusion. By means of a physical property of the resulting PDE model, a decoupled multiscale solution strategy can be derived, where each linear problem is approximated by finite element methods. A numerical investigation illustrates a clear impact of spatial effects on the separatrix of the PDE model. We use non-intrusive methods from the field of uncertainty quantification to conduct a sensitivity analysis of the most uncertain model parameters, enabling us to quantify this impact.

1 Introduction

Cell-to-cell communication plays a key role in multiple inflammatory processes and immune responses. Immune cells need to communicate across spatial and temporal scales in order to eliminate invading patogens or reduce abnormal inflammation as in fibrosis. Understanding the different factors that affect this cell-to-cell communication becomes crucial if one wants to enhance the immune response in order to eliminate the pathogens, or reduce the immune response in the case of abnormal inflammation. Immune cells mainly communicate by cytokines signaling.

We study the two-cell circuit formed by fibroblasts and macrophages, as these two cell types exist in most mammalian tissues and perform a typical homeostatic mechanism. The topology of the cell circuit we consider is that of [9], where sufficient conditions on stability were determined. As seen in figure 1, these are the imposition of a carrying capacity that constrains the total number of fibroblasts and growth factor regulation by negative feedback. The latter process is modeled as auto-regulation (endocytosis), where one cell type consumes the cytokine that the other produces. Our contribution is an investigation an extended model. The original ODE two-cell circuit of [9] is augmented by terms modeling random cell migration, chemotaxis and molecular diffusion. Cell migration is assumed to follow a diffusive process whereas chemotaxis constitutes directed motion towards the cell type's associated growth factor.

This paper is structured as follows. We first introduce the mathematical model formulation and explain its physical parameters and the numerical simulation methods. This is followed by a discussion of exemplary simulations of the resulting PDE model and computation of its separatrix for spatially heterogeneous and homogeneous initial conditions. Afterwards, we quantify the influence of the most uncertain model parameters on state transitions in the PDE model. Finally, the conclusion summarizes our findings.

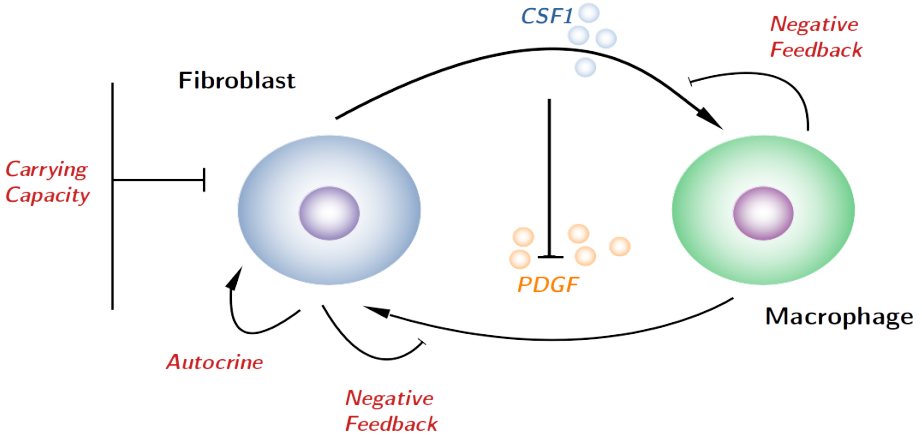

Figure 1: Growth-factor dependent cell circuit between macrophages and fibroblasts.

2 PDE Model

2.1 Mathematical Model

The evolution of cell concentration of fibroblats and macrophages, as well as the molecule concentration of growth factors can be described by a set of partial differential equations (PDEs). For the sake of simplicity, we use the standard notations for this paper, as $L^p(\Omega)$ for Lebesgue spaces, and $W^{k,p}(\Omega)$, $H^k(\Omega) = W^{k,2}(\Omega)$ for Sobolev spaces.

$$\frac{\partial F}{\partial t} = D_F \Delta F - \eta_1 \nabla \cdot (F \nabla P) + l_1 (\frac{P}{k_1 + P}) F (1 - \frac{F}{K}) - m_1 F \quad \text{in } (0,T] \times \Omega\,, \tag{1a}$$

$$\frac{\partial M}{\partial t} = D_M \Delta M - \eta_2 \nabla \cdot (M \nabla C) + l_2 (\frac{C}{k_2 + C}) M - m_2 M \quad \text{in } (0,T] \times \Omega\,, \tag{1b}$$

$$\frac{\partial C}{\partial t} = D_1 \Delta C + b_1 F - \frac{a_1 M C}{k_2 + C} - g_1 C \quad \text{in } (0,T] \times \Omega\,, \tag{1c}$$

$$\frac{\partial P}{\partial t} = D_2 \Delta P + b_2 M + b_3 F - \frac{a_2 F P}{k_1 P} - g_2 P \quad \text{in } (0,T] \times \Omega\,. \tag{1d}$$

Here F and M are the concentration of fibroblasts and macrophages, C and P represent the concentration of colony-stimulating factor (CSF) and platelet-derived growth factor (PDGF), respectively. $T > 0$ is the final time, $\Omega \in \mathbb{R}^d, d = \{2, 3\}$ is a bounded domain with a Lipschitz-continuous boundary. The physical meaning of each term in Equation (1) are summarized in Table 1, and the physical parameters appear in Equation (1) are listed in Table 2. Equation (1) contains the same reaction terms as the ODE system described in [9], combined with a two-species, two-stimulant chemotaxis model [8]. We impose homogeneous Neumann boundary conditions for all four variables as we want to avoid a flux of cells or molecules over the boundary $\partial\Omega$.

Migration:	$D_F \Delta F$, $D_M \Delta M$.	Chemotaxis:	$\eta_1 \nabla \cdot (F \nabla P)$, $\eta_2 \nabla \cdot (M \nabla C)$.
Proliferation:	$l_1(\frac{P}{k_1+P})F$, $l_2(\frac{C}{k_2+C})M$	Saturation:	$-l_1(\frac{P}{k_1+P})\frac{F^2}{K}$.
Removal:	$m_1 F$, $m_2 M$.	Diffusion:	$D_1 \Delta C$, $D_2 \Delta P$.
Secretion:	$b_1 F$, $b_2 M$, $b_3 F$.	Endocytosis:	$-\frac{a_1 M C}{k_2+C}$, $-\frac{a_2 F P}{k_1+P}$.
Degradation:	$-g_1 C$, $-g_2 P$.		

Table 1: Physical meaning of each term in the partial differential model.

l_1, l_2	maximal proliferation rate of fibroblasts and macrophages
m_1, m_2	removal rate of cells
K	carry capacity of fibroblasts
k_1, k_2	binding affinity of growth factor CSF and PDGF
a_1	maximal endocytosis rate of CSF by macrophages
a_2	maximal endocytosis rate of PDGF by fibroblasts
b_1	CSF secretion rate of fibroblasts
b_2	PDGF secretion macrophages
b_3	PDGF secretion rate of fibroblasts
g_1, g_2	degradation rate
D_1, D_2	cytokine diffusion coefficient
D_F, D_M	diffusion coefficient of fibroblasts and macrophages mobility
η_1, η_2	chemotactic coefficient

Table 2: Summary of physical parameters in considered mathematical model.

2.2 Numerical Method

We consider the finite element method (FEM) to solve the considered coupled PDEs. Equation (1) has to be transformed into the weak form, it implies that we multiply Equation (1) with test functions v from an appropriate space V and apply integration by parts. Under the framework of the finite element method, the space V^h is precisely a finite dimensional space $V^h \subset V$. The weak formulation for the fibroblast-macrophage evolution model reads as:

Find $u := (F, M, C, P)^T \in U := V^4$ such that

$$(\frac{\partial F}{\partial t}, v_F) + (D_F \nabla F, \nabla v_F) - (\eta_1 F \nabla P, \nabla v_F) - (l_1(\frac{P}{k_1 + P})F(1 - \frac{F}{K}), v_F) + (m_1 F, v_F) = 0 \tag{2a}$$

$$(\frac{\partial M}{\partial t}, v_M) + (D_M \nabla M, \nabla v_M) - (\eta_2 M \nabla C, \nabla v_M) - (l_2(\frac{C}{k_2 + C})M, v_M) + (m_2 M, v_M) = 0 \tag{2b}$$

$$D_1(\nabla C, \nabla v_C) - (b_1 F, v_C) + (\frac{a_1 MC}{k_2 + C}, v_C) + (g_1 C, v_C) = 0 \tag{2c}$$

$$D_2(\nabla P, \nabla v_P) - (b_2 M, v_P) - (b_3 F, v_P) + (\frac{a_2 FP}{k_1 + P}, v_P) + (g_2 P, v_P) = 0 \tag{2d}$$

for all test functions $v_F, v_M, v_C, v_P \in V_0$ such that $V_0 := \{v \in V : v|_{\partial\Omega} = 0\}$.

In equations (2c, 2d), we assume $\frac{\partial C}{\partial t} = 0 = \frac{\partial P}{\partial t}$ as the process of molecular diffusion is much faster than that of cell migration and thus takes place on a larger time scale. For the remaining time derivatives, we apply a θ-scheme with $\theta = 0.5$ (Crank-Nicolson method). To resolve the coupling between the cell equations and the cytokine equations, we utilize a decoupled, sequential solution strategy in each time step.

1. Using $(F^{k-1}, M^{k-1})^T$, apply a nonlinear solver to the cytokine equations, giving $(C^k, P^k)^T$.
2. Using $(C^k, P^k)^T$, apply a nonlinear solver to the cell equations, giving $(F^k, M^k)^T$.

Here $(F^0, M^0)^T$ are simply the initial cell concentrations. All nonlinear systems are treated with an inexact Newton's method using the Eisenstat-Walker strategy [3].

3 Numerical Results

For our numerical tests, the computational domain is set to a 2D square, $\Omega = [L \times L]$, $L = 35\,000\,\mu\text{m}$, because its area is approximately equal to the area of the cell-culture dish which is used in the experiment.

3.1 Initial Conditions

The initial conditions have to be defined before solving Equation (1). The initial values of colony-stimulating factors and platelet-derived growth factors are set to 0, which corresponds the experimental setting. The initial condition for fibroblasts and macrophages is defined by a shape of Gaussian distribution:

$$F(x,y,0) = A_F \exp(-\frac{(x-x_F)^2}{2r^2} - \frac{(y-y_F)^2}{2r^2}) \,, \tag{3a}$$

$$M(x,y,0) = A_M \exp(-\frac{(x-x_M)^2}{2r^2} - \frac{(y-y_M)^2}{2r^2}) \,, \tag{3b}$$

where (x_F, y_F) and (x_M, y_M) are the center of the Gaussian distributions for fibroblasts and macrophages. r is the standard deviation of Gaussian distribution and is used in our model to control the size of the distribution. A_F and A_M define the concentration of initial state.

3.2 Separatrix

The separatrix is a boundary between states with distinct dynamic behavior in a system of differential equations. In [9], the authors used an analytical screening approach with an ordinary differential model of two-cell circuits [1] to show that in regards to different range of initial conditions for fibroblasts and macrophages there exist three states: "ON", "OFF" and "ON-OFF". "ON" state represents the concentration of fibroblasts and macrophages flow to a stable coexistence. "OFF" state means that the concentration of the two cell types decays to zero. "ON-OFF" state signifies the unstable state, where one cell's concentration increases, and another decreases to zero.

For our numerical studies, we focus on the separatrix of the two stable states as mentioned above. We investigate the how spatial relations between fibroblasts and macrophages can effect the on the separatrix on stable states by using the partial differential model (Equation (1)).

3.3 Spatial Effect on Separatrix

Concerning the spatial influence on the separatrix, the phase portrait calculate by the model based ordinary differential equations (ODE) is considered as the reference results in this study. The ordinary differential model is formulated as follows:

$$\frac{dF}{dt} = l_1(\frac{P}{k_1+P})F(1-\frac{F}{K}) - m_1 F \,, \tag{4a}$$

$$\frac{dM}{dt} = l_2(\frac{C}{k_2+C})M - m_2 M \,, \tag{4b}$$

$$\frac{dC}{dt} = b_1 F - \frac{a_1 MC}{k_2+C} - g_1 C \,, \tag{4c}$$

$$\frac{dP}{dt} = b_2 M + b_3 F - \frac{a_2 FP}{k_1 P} - g_2 P\Omega \,. \tag{4d}$$

The physical parameters here are the same as in Equation (1).

Two different types of initial conditions are studied: homogeneous and inhomogeneous initial condition. The homogeneous initial condition is used to mimic the initial condition in the ordinary differential model (Equation (4)), where no spatial relation on fibroblasts and macrophages plays a role. The inhomogeneous initial condition is represented by Equation (3), the spatial relation between F and M is characterized by the radius r and the density A_F and A_M.

Figure 2 shows the separatrix computed by the PDE model (Equation (1)) taking into account of two types of initial condition comparing with the phase portrait obtained from ODE model. The inhomogeneous initial condition is set to $d = 12\,000\,\mu\text{m}$ and $r = 2500\,\mu\text{m}$. The red line is the separatrix,

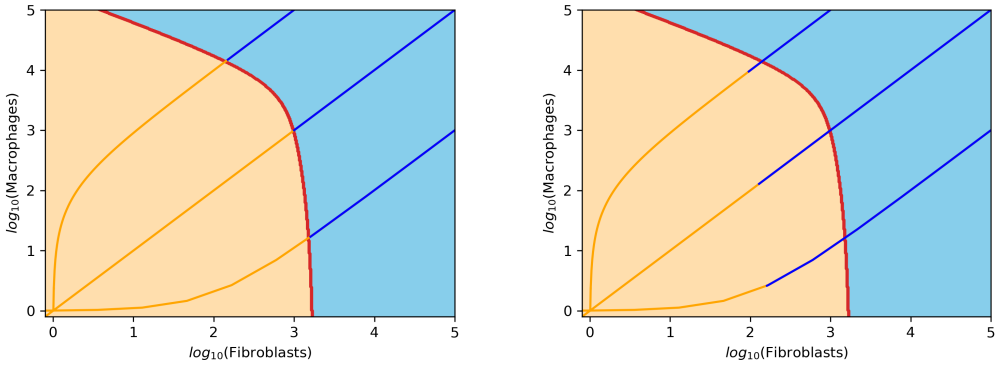

(a) Homogeneous initial condition. **(b)** Inhomogeneous initial condition.

Figure 2: Comparison of separatrix for homogeneous and inhomogeneous initial condition, $d = 12\,000\,\mu\text{m}$, $r = 2500\,\mu\text{m}$.

Parameter	Value	Parameter	Value
l_1	$0.9\,\text{D}^{-1}$	l_2	$0.8\,\text{D}^{-1}$
m_1, m_2	$0.3\,\text{D}^{-1}$	K	1.0×10^6 Ce
a_1	1.3536×10^6 Mo/Ce/D	a_2	7.344×10^5 Mo/Ce/D
b_1	6.768×10^5 Mo/Ce/D	b_2	1.008×10^5 Mo/Ce/D
b_3	3.56×10^5 Mo/Ce/D	k_1	1.8×10^8 Mo
k_2	2.3×10^8 Mo	g_1, g_2	$1.92\,\text{D}^{-1}$
D_1, D_2	$8.64 \times 10^6\,\mu\text{m}^2/\text{D}$	η_1	$72\,\mu\text{m}^2/\text{D/Mo}$
η_2	$144\,\mu\text{m}^2/\text{D/Mo}$	D_F	$146.9\,\mu\text{m}^2/\text{D}$
D_M	$4.752\,\mu\text{m}^2/\text{D}$		

* D: days. Ce: cells. Mo: molecules.

Table 3: Physical parameters used in PDE model.

and the yellow and blue areas are obtained by the ODE model (Equation (4)), the x- and y-axis are the initial values for fibroblasts and macrophages, respectively. The yellow region represents the "OFF" state, meaning with these initial values, the concentration of fibroblasts and macrophages will decay to zero. The blue region represents the "ON" state, where the concentration of fibroblasts and macrophages will remain constant after certain period of time. As the computation of PDE model is much more time consuming than ODE model, we only study three trajectories of two stable states per each different initial conditions (i.e. per each combination of d and r) which are $C_M = C_F$, $C_M = 0.01 \times C_F + 1$ and $C_M = 100 \times C_F - 100$, here, C_F and C_M mean the initial concentration of fibroblasts and macrophages.

In Figure 2a, the numerical results with homogeneous initial condition agrees with the ODE model, because the homogeneous initial condition imitates the computation setting in ODE model, and there is no spatial impact. However, when separating the centers of cell cultures for fibroblasts and macrophages in the initial condition (Figure 3), the separatrix becomes smaller than the separatrix defined by ODE model (Figure 2b).

Figures 3 to 5 are the simulation snapshots of the PDE model for a period of 30 days with inhomogeneous initial condition, where $d = 12\,000\,\mu\text{m}$, $r = 2500\,\mu\text{m}$, $C_F = C_M = 1 \times 10^4$ Cells. As described earlier, only the concentration of fibroblasts and macrophages are defined for the initial condition, CSF and FPDG are set to zero (Figure 3). After 15 days cell culture of fibroblasts and macrophages move towards each other, CSF and PDGF are also generated (Figure 4). One can observe that macrophages

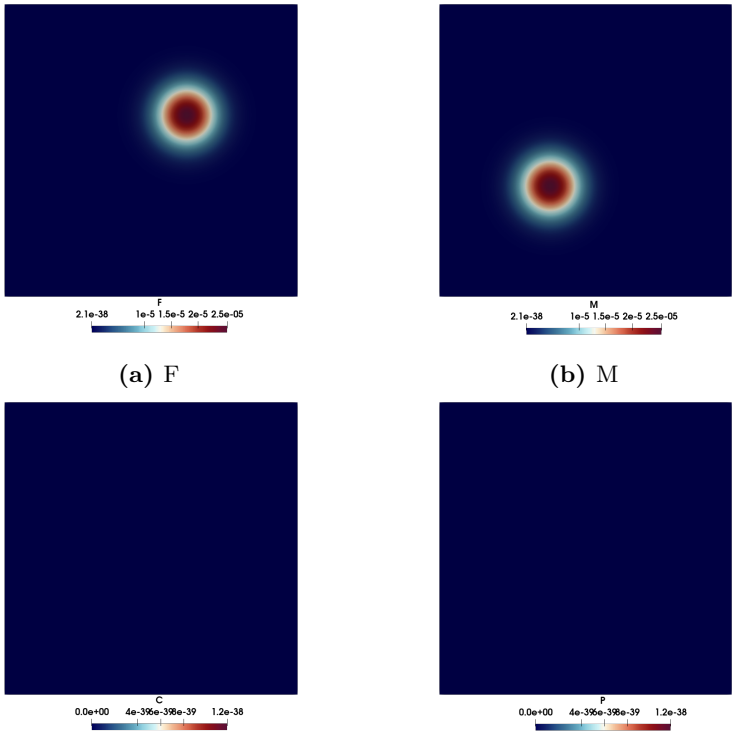

(a) F **(b)** M

(c) CSF **(d)** PDGF

Figure 3: Numerical results of PDE model with inhomogeneous initial condition, $d = 12\,000\,\mu\text{m}$, $r = 2500\,\mu\text{m}$. Day 0.

move much faster than fibroblasts because its chemotactic coefficient is twice larger than fibroblasts. The "ON" state is reached after a longer period of time (Figure 5), fibroblasts and macrophages associated at high concentration of both cells.

Table 4 summarizes the initial values of fibroblasts on three trajectories, where the separatrix is found for PDE and ODE model. For the PDE model, the spatial relationship between fibroblasts and macrophages cell cultures in the initial condition is characterized by varying r and d in Equation (3). First, we observe the separatrix of PDE model is always smaller than those defined by ODE model, in other words, the "ON" state is attained with smaller amount of cell for the initial condition. One also needs the higher cell concentration to reach the "ON" state, when the distance between two cell clusters is larger. The larger radius r means the cell concentration is lower for the same initial value, thus the higher initial value is required for reaching the same separatrix. In accordance with these three trajectories, the cell concentration of macrophages seems to be more important, if there exists considerable amount of macrophages, then the initial value of fibroblasts does not have to be very large, the two-cell system can still reach the stable state.

4 Global Sensitivity Analysis with Polynomial Chaos Expansion

The global sensitivity analysis (GSA) [5] is a process of studying the respective impact of input uncertain parameters on model outputs. The variance-based sensitivity analysis, i.e. Sobol's indices [6], has received much attention since it can provide accurate information for most models.

Sobol' indices are an important tool to establish an importance ranking of input parameters and their interactions

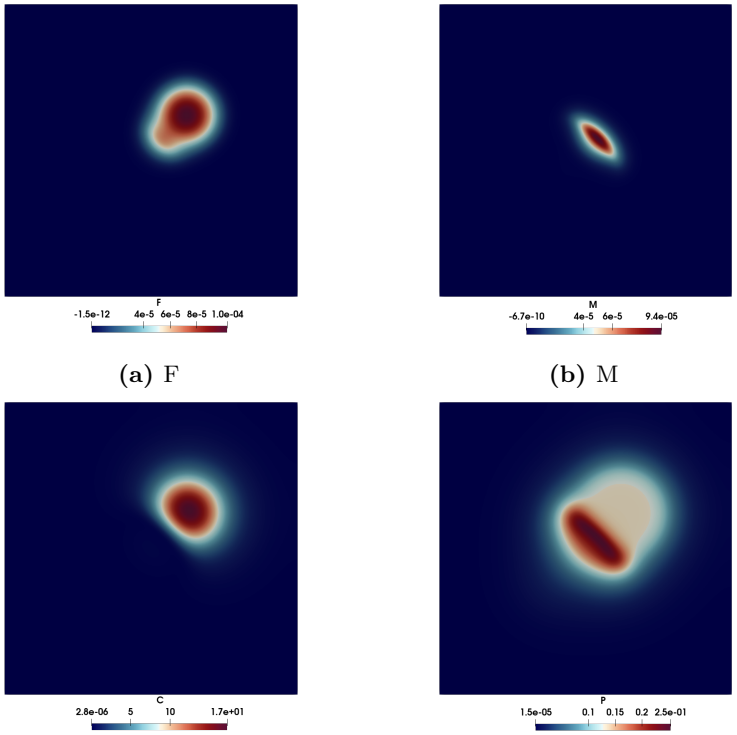

(a) F **(b)** M

(c) CSF **(d)** PDGF

Figure 4: Numerical results of PDE model with inhomogeneous initial condition, $d = 12\,000\,\mu\text{m}$, $r = 2500\,\mu\text{m}$. Day 15.

Trajectory	$r = 2500$				ODE
	$d = 0$	$d = 4000$	$d = 8000$	$d = 12000$	
$C_M = C_F$	84.5	95.8	128.7	140.5	954.9
$C_M = 0.01 \times C_F + 1$	116.7	128.7	139.1	161.7	1513.5
$C_M = 100 \times C_F - 100$	12.7	16.3	31.9	95.8	102.3
Trajectory	$r = 5000$				ODE
	$d = 0$	$d = 4000$	$d = 8000$	$d = 12000$	
$C_M = C_F$	217.8	227.5	260.5	293.4	954.9
$C_M = 0.01 \times C_F + 1$	298.8	326.3	359.3	369.7	1513.5
$C_M = 100 \times C_F - 100$	32.5	35.4	43.2	62.8	102.3
Trajectory	$r = 7500$				ODE
	$d = 0$	$d = 4000$	$d = 8000$	$d = 12000$	
$C_M = C_F$	416.6	425.2	445.2	491.1	954.9
$C_M = 0.01 \times C_F + 1$	543.3	553.2	570.7	598.1	1513.5
$C_M = 100 \times C_F - 100$	62.8	64.9	71.5	81.7	102.3

Table 4: Initial value of fibroblast of separatrices for three trajectories from PDE and ODE model with different initial condition.

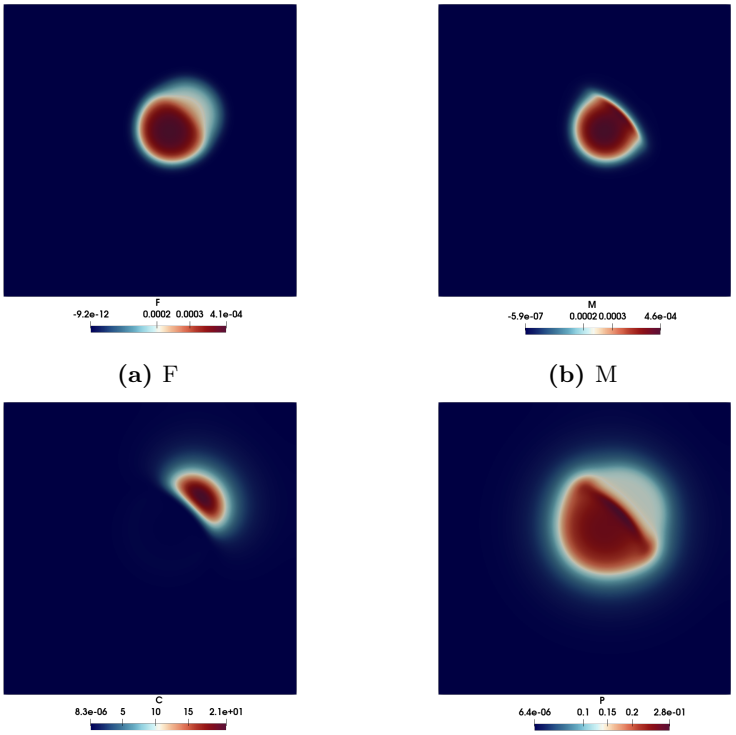

(a) F **(b)** M

(c) CSF **(d)** PDGF

Figure 5: Numerical results of PDE model with inhomogeneous initial condition, $d = 12\,000\,\mu\text{m}$, $r = 2500\,\mu\text{m}$. Day 30.

4.1 Variance-Based Method

The variance-based method aims to decompose the variance of model outputs as a sum of contribution from each uncertain input variable, it is also referred as ANOVA technique, which stands for "Analysis Of Variance". Let us consider first a model f with M uncertain input parameters $\boldsymbol{\xi} = \{\xi_1, \xi_2, ..., \xi_M\}$, and the output y:

$$y = f(\boldsymbol{\xi})\,. \tag{5}$$

Assuming $\boldsymbol{\xi}$ are mutually independent and f is square-integrable with respect to associated probability measure, the Sobol' decomposition of Equation (5) has the following form in summands of increasing dimension [6]:

$$f(\boldsymbol{\xi}) = f_0 + \sum_{i=1}^{M} f_i(\xi_i) + \sum_{i \le j}^{M} f_{i,j}(\xi_i, \xi_j) + \cdots + f_{1,2,\ldots,M}(\boldsymbol{\xi})\,, \tag{6}$$

or equivalently

$$f(\boldsymbol{\xi}) = f_0 + \sum_{\boldsymbol{\beta} \neq \emptyset} f_{\boldsymbol{\beta}}(\boldsymbol{\xi}_{\boldsymbol{\beta}})\,, \tag{7}$$

where f_0 is the expected value of y, $\boldsymbol{\beta} = \{i_1, ..., i_s\} \subseteq \{1, ..., M\}$ are multivariate index sets, $\boldsymbol{\xi}_{\boldsymbol{\beta}}$ is a subset of $\boldsymbol{\xi}$ containing the components indexed in $\boldsymbol{\beta}$. In other words, the total number of summands in Equation (7) is $2^M - 1$. This decomposition is uniquely defined if $f_{i_1,\ldots,i_s}(\xi_{i_1}, ..., \xi_{i_s})$ with $\{i_1, ..., i_s\} \subseteq \{1, ..., M\}$ are orthogonal functions, i.e.

$$\int f_{\boldsymbol{\beta}_1}(\boldsymbol{\xi}_{\boldsymbol{\beta}_1}) f_{\boldsymbol{\beta}_2}(\boldsymbol{\xi}_{\boldsymbol{\beta}_2}) d\boldsymbol{\xi} = 0, \qquad \boldsymbol{\beta}_1 \neq \boldsymbol{\beta}_2\,. \tag{8}$$

The variances of y are defined by

$$V_{\boldsymbol{\beta}} = V_{i_1,\ldots,i_s} = \int f^2_{i_1,\ldots,i_s} d\xi_{i_1} \ldots d\xi_{i_s} \,, \tag{9}$$

and

$$V_T = \int f^2(\boldsymbol{\xi}) d\boldsymbol{\xi} - f_0^2 \,, \tag{10}$$

$$= \sum_{i=1}^{M} V_i + \sum_{j>1}^{M} V_{i,j} + \cdots + V_{1,\ldots,M} \tag{11}$$

denotes the total variance of $f(\boldsymbol{\xi})$. V_i is the partial variance according to random input ξ_i itself, $V_{i_1,\ldots,i_s}$ is the partial variance defining by the interactions between random inputs $\{\xi_{i_1}, \ldots, \xi_{i_s}\} \subseteq \{\xi_1, \ldots, \xi_M\}$. The variance-based Sobol's sensitivity indices can be then defined:

$$S_{\boldsymbol{\beta}} = S_{i_1,\ldots,i_s} = \frac{V_{i_1,\ldots,i_s}}{V_T} = \frac{V_{\boldsymbol{\beta}}}{V_T} \,. \tag{12}$$

The Sobol's indices quantify the contribution of random input parameters on the output variance. The higher value of Sobol's index means the random input or the interplay between random inputs introduces more uncertainty into the system. Moreover, the first order sensitivity index is defined by:

$$S_i = \frac{V_i}{V_T} \,, \tag{13}$$

which quantify the additive effect of each input parameter on the response variability separately. The second order sensitivity index is defined as:

$$S_{ij} = \frac{V_{ij}}{V_T} \,, \tag{14}$$

which expresses the amount of variance of $f(\boldsymbol{\xi})$ explained by the interaction between ξ_i and ξ_j.

4.2 Polynomial Chaos Expansion

The square-integrable random response $f(\boldsymbol{\xi})$ in Equation (5) have the following polynomial chaos (PC) expansion [7]:

$$f(\boldsymbol{\xi}) = \sum_{\substack{|\boldsymbol{\alpha}|=0 \\ \boldsymbol{\alpha} \in \mathbb{N}^M}}^{\infty} c_{\boldsymbol{\alpha}} \Psi_{\boldsymbol{\alpha}}(\boldsymbol{\xi}) \,, \tag{15}$$

where $\boldsymbol{\alpha} = \{\alpha_1, \ldots, \alpha_M\}$ is the multi-index, α_i is a non-negative integer that specifies the order of univariate basis polynomial, and $|\boldsymbol{\alpha}| = \sum_{i=1}^{M} \alpha_i$. $c_{\boldsymbol{\alpha}}$ are the stochastic modes of $f(\boldsymbol{\xi})$, the multivariate orthonormal polynomial $\Psi_{\boldsymbol{\alpha}}(\boldsymbol{\xi})$ is defined by a tensor product of 1D polynomials and reads:

$$\Psi_{\boldsymbol{\alpha}}(\boldsymbol{\xi}) = \prod_{i=1}^{M} \psi_{\alpha_i}(\xi_i) \,, \tag{16}$$

where $\psi_{\alpha_i}(\xi_i)$ is the univariate orthonormal polynomial of degree α_i in ξ_i, $\psi(\xi)$ is chosen regarding the probability distribution of ξ.

The orthogonality of $\Psi_{\boldsymbol{\alpha}}$ is defined with respect to $\boldsymbol{\xi}$, i.e.

$$\int_{\Omega^M} \Psi_{\boldsymbol{\alpha}_1}(\boldsymbol{\xi}) \Psi_{\boldsymbol{\alpha}_2}(\boldsymbol{\xi}) \rho(\boldsymbol{\xi}) d\boldsymbol{\xi} = 0 \,, \qquad \boldsymbol{\alpha}_1 \neq \boldsymbol{\alpha}_2 \,, \tag{17}$$

where $\rho(\boldsymbol{\xi})$ is joint probability density function of $\boldsymbol{\xi}$.

For the computational convenience, Equation (15) needs to be approximated with a truncated series:

$$f(\boldsymbol{\xi}) \simeq \sum_{|\boldsymbol{\alpha}|=0}^{p} c_{\boldsymbol{\alpha}} \Psi_{\boldsymbol{\alpha}}(\boldsymbol{\xi}) = \sum_{i=0}^{P} c_i \Psi_i(\boldsymbol{\xi}) \,, \tag{18}$$

where p is the truncated total polynomial order, P is the total stochastic modes depending on p and the number of uncertain parameters M,

$$P + 1 = \frac{(M+p)!}{M!p!} \,. \tag{19}$$

4.3 Sparse Grid Numerical Integration

The purpose of applying the polynomial chaos expansion technique is to obtain the coefficients C_i in Equation (18), such the stochastic moments of quantities of interest can be calculated. Taking the inner product of the output of PC expansion with $\Psi_k(\boldsymbol{\xi})$ based on the orthogonality of chaos basis, it reads

$$C_k = \frac{\langle f(\boldsymbol{\xi}), \Psi_k(\boldsymbol{\xi}) \rangle}{\langle \Psi_k(\boldsymbol{\xi}), \Psi_k(\boldsymbol{\xi}) \rangle} \,, \quad \forall k \,. \tag{20}$$

Therefore, determining the chaos polynomial coefficients reduces to computing the following integral:

$$I_k = \int_{\Omega^M} f(\boldsymbol{\xi}) \Psi_k(\boldsymbol{\xi}) \rho(\boldsymbol{\xi}) d\boldsymbol{\xi} \,, \tag{21}$$

where, $\rho(\boldsymbol{\xi})$ is again joined probability density function. The sparse grid interpolation is used as the numerical integration scheme for the calculation of the equation above.

4.4 PC-based Sensitivity Functions

Due to the orthogonality of the basis and linearity of polynomial chaos expansion, we can reorder Equation (18) in order to separate the contribution of each parameter ξ_i as in Equation (6). Let us rewrite Equation (18) as

$$f(\boldsymbol{\xi}) = \sum_{|\boldsymbol{\alpha}|=0}^{p} c_{\boldsymbol{\alpha}} \Psi_{\boldsymbol{\alpha}}(\boldsymbol{\xi}) = \sum_{\boldsymbol{\alpha} \in \mathcal{A}} c_{\boldsymbol{\alpha}} \Psi_{\boldsymbol{\alpha}}(\boldsymbol{\xi}) \,, \tag{22}$$

then we can define intersection sets with $\boldsymbol{\beta}$ in Equation (7):

$$\mathcal{A}_{\boldsymbol{\beta}} = \{ \boldsymbol{\alpha} \in \mathcal{A} : k \in \boldsymbol{\beta} \Leftrightarrow \alpha_k \neq 0 \} \,. \tag{23}$$

The PC-based Sobol' indices can be obtained by

$$S_{\boldsymbol{\beta}} = \frac{V_{\boldsymbol{\beta}}}{V_T} = \frac{\sum_{\boldsymbol{\alpha} \in \mathcal{A}_\beta} c_{\boldsymbol{\alpha}}^2}{\sum_{\boldsymbol{\alpha} \in \mathcal{A}} c_{\boldsymbol{\alpha}}^2} \,. \tag{24}$$

Therefore, computing the Sobol' indices by using PC expansion as a surrogate model is to determine the coefficient of chaos polynomials in Equation (18). There exist two distinguished methods for calculating the coefficient of calculate c_i: the intrusive and non-intrusive methods. In this paper, we use the non-intrusive method, more precisely the stochastic Sparse-Grids method [2, 4], because we can use the numerical model described in the last section as a black box, and compute the indices as a post-processing step from model evaluations.

Our quantity of interest is the point on the separatrix given by the trajectory $N_F = N_M$ for inhomogeneous initial conditions. The parameter distributions are shown in table 5. As seen in the second order indices of figure 6, the separatrix exhibits sensitivity to all four parameters under consideration. The binding affinity k_1 is almost exactly proportional to the separatrix, which explains its large index. The radius of the populations determines the cell density, which in turn for a smaller radius also increases the growth factor density. Thus, a smaller radius leads to a decreased separatrix. The sensitivity to k_2 is lower than that of k_1; the macrophage growth rate therefore does not appear to significantly drive the

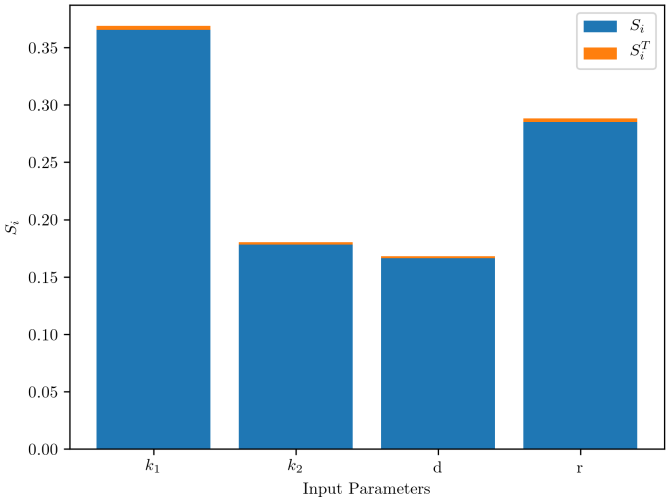

Figure 6: Total Sobol' indices S_i^T in orange, the first-order Sobol' indices S_i in blue.

separatrix. For this trajectory, it can also be established that d is the least significant parameter. This may be explained by the macrophage populations nearly always reaching their fibroblast-produced growth factor before vanishing, even for large distances. For all indices, second-order interactions are much less significant than first-order effects.

Parameter	Distribution
k_1	$\mathcal{U}(1.8 \times 10^7\,\mathrm{Mo}, 1.8 \times 10^9\,\mathrm{Mo})$
k_2	$\mathcal{U}(2.3 \times 10^7\,\mathrm{Mo}, 2.3 \times 10^9\,\mathrm{Mo})$
r	$\mathcal{U}(2000\,\mu\mathrm{m}, 7500\,\mu\mathrm{m})$
d	$\mathcal{U}(0\,\mu\mathrm{m}, 10\,000\,\mu\mathrm{m})$

Table 5: Parameter distributions for the sensitivity analysis.

5 Conclusion and Outlook

In this work, we conducted the first investigation of a PDE model that represents a spatially heterogeneous two-cell circuit. Using a multiscale numerical approach, we found that the PDE model accurately captures the results of a previously published ODE model for homogeneous initial data. We also found that its separatrix for heterogeneous initial conditions is lower than that of the homogeneous case. This is due to the homogeneous initial conditions having the lowest possible local cell concentration: The cell concentration immediately dictates the growth factor concentration, and lower growth factor concentration due to lower cell concentration thus increases the separatrix. Our sensitivity analysis of the separatrix found that in the set of uncertain model parameters, the binding affinity of PDGF is clearly most important as it determines the growth rate of fibroblasts. There is also a large sensitivity to the radius of the cell populations since it is inversely proportional to the cell concentration and thus cytokine concentration. The separatrix does not exhibit large sensitivity to the binding affinity of CSF, neither does the distance between fibroblast and macrophage populations appear to have a strong impact. Thus, while there is a quantifiable spatial effect on the separatrix, the radius of the cell populations appears to account for most of it.

Acknowledgements

The authors acknowledge the support by Informatics for Life project funded by the Klaus Tschira Foundation, the state of Baden-Württemberg through bwHPC and the German Research Foundation (DFG) through grant INST 35/1134-1 FUGG, and Heidelberg Institute for Theoretical Studies (HITS).

References

[1] Miri Adler et al. "Endocytosis as a stabilizing mechanism for tissue homeostasis". In: *Proceedings of the National Academy of Sciences* 115.8 (2018), E1926–E1935. ISSN: 0027-8424. DOI: 10.1073/pnas.1714377115. eprint: https://www.pnas.org/content/115/8/E1926.full.pdf. URL: https://www.pnas.org/content/115/8/E1926.

[2] Hans-Joachim Bungartz and Michael Griebel. "Sparse grids". In: *Acta numerica* 13.1 (2004), pp. 147–269.

[3] Stanley C Eisenstat and Homer F Walker. "Choosing the forcing terms in an inexact Newton method". In: *SIAM Journal on Scientific Computing* 17.1 (1996), pp. 16–32.

[4] Thomas Gerstner and Michael Griebel. "Numerical integration using sparse grids". In: *Numerical algorithms* 18.3-4 (1998), p. 209.

[5] Bryan E. Shepherd. "Global Sensitivity Analysis. The Primer by SALTELLI, A., RATTO, M., ANDRES, T., CAMPOLONGO, F., CARIBONI, J., GATELLI, D., SAISANA, M., and TARANTOLA, S." In: *Biometrics* 65.4 (2009), pp. 1311–1312. DOI: https://doi.org/10.1111/j.1541-0420.2009.01343_7.x. eprint: https://onlinelibrary.wiley.com/doi/pdf/10.1111/j.1541-0420.2009.01343_7.x. URL: https://onlinelibrary.wiley.com/doi/abs/10.1111/j.1541-0420.2009.01343_7.x.

[6] I.M Sobol. "Global sensitivity indices for nonlinear mathematical models and their Monte Carlo estimates". In: *Mathematics and Computers in Simulation* 55.1 (2001). The Second IMACS Seminar on Monte Carlo Methods, pp. 271 –280. ISSN: 0378-4754. DOI: https://doi.org/10.1016/S0378-4754(00)00270-6. URL: http://www.sciencedirect.com/science/article/pii/S0378475400002706.

[7] Dongbin Xiu. *Numerical Methods for Stochastic Computations: A Spectral Method Approach*. Princeton University Press, 2010. ISBN: 9780691142128. URL: http://www.jstor.org/stable/j.ctv7h0skv.

[8] Pan Zheng, Chunlai Mu, and Xuegang Hu. "Persistence property in a two-species chemotaxis system with two signals". In: *Journal of Mathematical Physics* 58.11 (2017), p. 111501.

[9] Xu Zhou et al. "Circuit Design Features of a Stable Two-Cell System". In: *Cell* 172.4 (2018), 744 –757.e17. ISSN: 0092-8674. DOI: https://doi.org/10.1016/j.cell.2018.01.015. URL: http://www.sciencedirect.com/science/article/pii/S0092867418300527.

Supplementary Materials

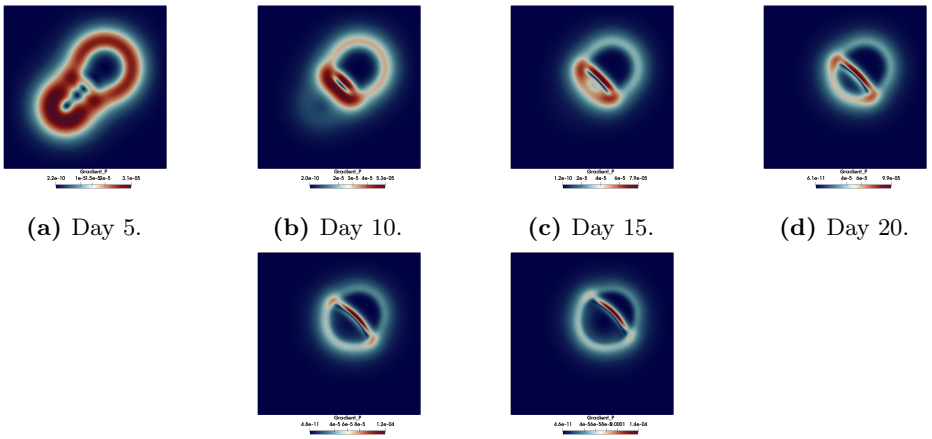

(a) Day 5. **(b)** Day 10. **(c)** Day 15. **(d)** Day 20.

(e) Day 25. **(f)** Day 30.

Figure 7: Magnitude of gradient from PDGF, from day 5 to day 30.

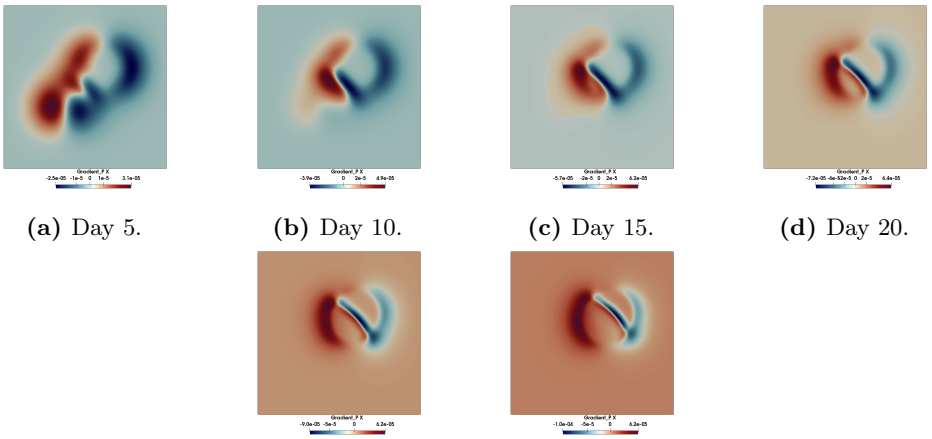

(a) Day 5. **(b)** Day 10. **(c)** Day 15. **(d)** Day 20.

(e) Day 25. **(f)** Day 30.

Figure 8: Gradient from PDGF in x direction, from day 5 to day 30.

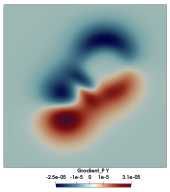

(a) Day 5.

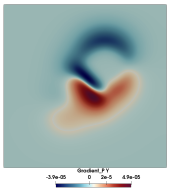

(b) Day 10.

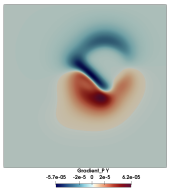

(c) Day 15.

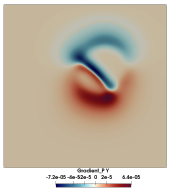

(d) Day 20.

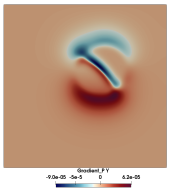

(e) Day 25.

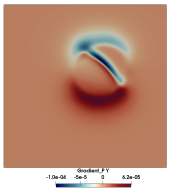

(f) Day 30.

Figure 9: Gradient from PDFG in y direction, from day 5 to day 30.

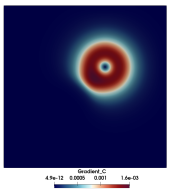

(a) Day 5.

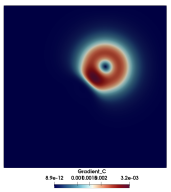

(b) Day 10.

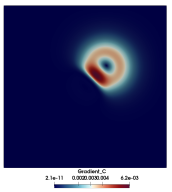

(c) Day 15.

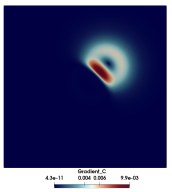

(d) Day 20.

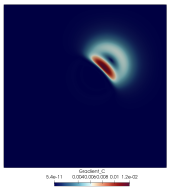

(e) Day 25.

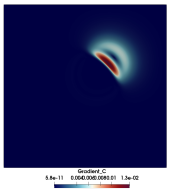

(f) Day 30.

Figure 10: Magnitude of gradient from CSF, from day 5 to day 30.

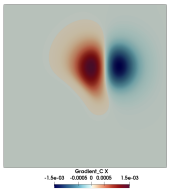

(a) Day 5.

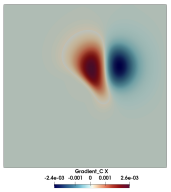

(b) Day 10.

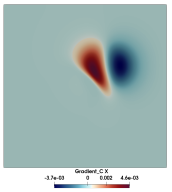

(c) Day 15.

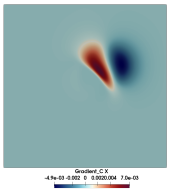

(d) Day 20.

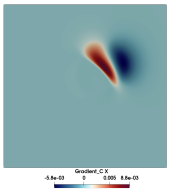

(e) Day 25.

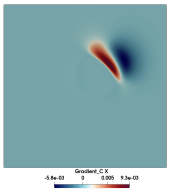

(f) Day 30.

Figure 11: Gradient from CSF in x direction, from day 5 to day 30.

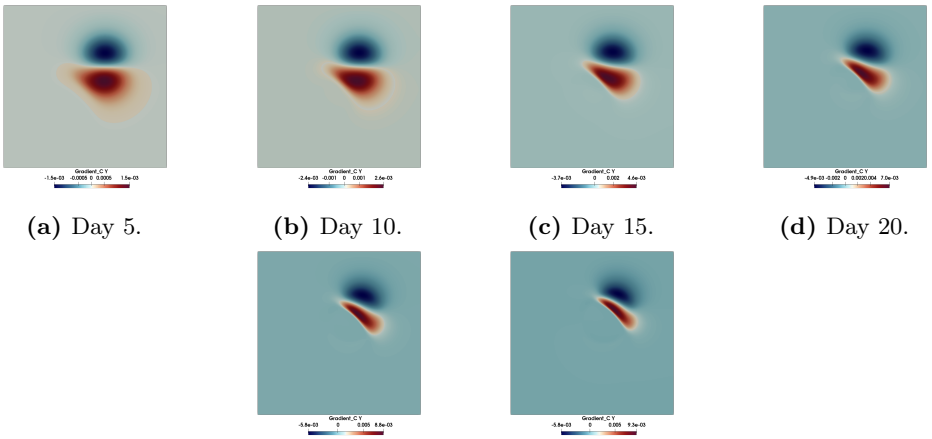

(a) Day 5. **(b)** Day 10. **(c)** Day 15. **(d)** Day 20.

(e) Day 25. **(f)** Day 30.

Figure 12: Gradient from CSF in x direction, from day 5 to day 30.

Preprint Series of the Engineering Mathematics and Computing Lab

recent issues

No. 2020-01 Saskia Haupt, Nassim Fard-Rutherford, Philipp D. Lösel, Lars Grenacher, Arianeb Mehrabi, Vincent Heuveline: Mathematical Clustering Based on CrossSections in Medicine: Application to the Pancreatic Neck

No. 2019-02 Nils Schween, Nico Meyer-H¨ubner, Philipp Gerstner, Vincent Heuveline: A time step reduction method for Multi-Period Optimal Power Flow problems

No. 2019-01 Philipp Gerstner, Martin Baumann, Vincent Heuveline: Analysis of the Stationary Thermal-Electro Hydrodynamic Boussinesq Equations

No. 2018-02 Simon Gawlok, Vincent Heuveline: Nested Schur-Complement Solver for a Low-Mach Number Model: Application to a Cyclone-Cyclone Interaction

No. 2018-01 David John, Michael Schick, Vincent Heuveline: Learning model discrepancy of an electric motor with Bayesian inference

No. 2017-06 Simon Gawlok, Philipp Gerstner, Saskia Haupt, Vincent Heuveline, Jonas Kratzke, Philipp Lösel, Katrin Mang, Maraike Schmidtobreick, Nicolai Schoch, Nils Schween, Jonathan Schwegler, Chen Song, Marin Wlotzka: HiFlow^3 Technical Report on Release 2.0

No. 2017-05 Nicolai Schoch, Vincent Heuveline: Towards an Intelligent Framework for Personalized Simulation-enhanced Surgery Assistance: Linking a Simulation Ontology to a Reinforcement Learning Algorithm for Calibration of Numerical Simulations

No. 2017-04 Martin Wlotzka, Thierry Morel, Andrea Piacentini, Vincent Heuveline: New features for advanced dynamic parallel communication routines in OpenPALM: Algorithms and documentation

No. 2017-03 Martin Wlotzka, Vincent Heuveline: An energy-efficient parallel multigrid method for multi-core CPU platforms and HPC clusters

No. 2017-02 Thomas Loderer, Vincent Heuveline: New sparsing approach for real-time simulations of stiff models on electronic control units

No. 2017-01 Chen Song, Markus Stoll, Kristina Giske, Rolf Bendl, Vincent Heuveline: Sparse Grids for quantifying motion uncertainties in biomechanical models of radiotherapy patients

No. 2016-02 Jonas Kratzke, Vincent Heuveline: An analytically solvable benchmark problem for fluid-structure interaction with uncertain parameters

No. 2016-01 Philipp Gerstner, Michael Schick, Vincent Heuveline, Nico Meyer-Hübner, Michael Suriyah, Thomas Leibfried, Viktor Slednev, Wolf Fichtner, Valentin Bertsch: A Domain Decomposition Approach for Solving Dynamic Optimal Power Flow Problems in Parallel with Application to the German Transmission Grid

No. 2015-04 Philipp Gerstner, Vincent Heuveline, Michael Schick : A Multilevel Domain Decomposition approach for solving time constrained Optimal Power Flow problems

No. 2015-03 Martin Wlotzka, Vincent Heuveline: Block-asynchronous and Jacobi smoothers for a multigrid solver on GPU-accelerated HPC clusters

Preprint Series of the Engineering Mathematics and Computing Lab (EMCL)

www.emcl.iwr.uni-heidelberg.de